Reversible radial deformation up to the complete flattening of carbon nanotubes in nanoindentation

Majid Minary-Jolandan and Min-Feng Yu[a)]
Department of Mechanical Science and Engineering, University of Illinois at Urbana-Champaign, 1206 West Green Street, Urbana, Illinois 61801, USA

(Received 6 November 2007; accepted 29 January 2008; published online 7 April 2008)

The reversible flattening up to 60% deformation of individual multiwalled carbon nanotubes (MWCNTs) was revealed with nanoindentation. The nanoindentation induced, in terms of indentation force versus indentation depth, two linear deformation responses and a nonlinear one in between in the measurement of an ~9 nm diameter MWCNT having six walls. A continuum shell model was applied and found to be fully capable of describing the observed behavior and extracting accurate mechanical properties of the MWCNT. The measured linear deformation persisted up to an indentation depth twice the shell thickness of the MWCNT, a behavior much like a macroscopic thin shell in classical shell theory. Nonlinear deformation was subsequently introduced due to the extended flattening of the MWCNT in the axial direction and the formation of high curvature "bulbs" along the edges of a squashed MWCNT. Finally, the elastic deformation of such bulbs initiated the second linear deformation response. The deformation behavior was found to be fully reversible, manifesting the remarkable mechanical performance of CNT as a nanoscale elastic shell in sustaining severe mechanical deformation. © *2008 American Institute of Physics*.
[DOI: 10.1063/1.2903438]

I. INTRODUCTION

Despite their extremely high tensile strength and Young's modulus in axial direction,[1] carbon nanotubes (CNTs) are shown to be rather soft in transversal (radial) direction.[2] In fact, it has been observed that van der Waals interaction alone between two adjacent multiwalled CNTs (MWCNTs) can induce radial deformation.[3] Knowledge about the transversal mechanical properties of CNTs is important for their use as light-weight fiber components in high performance composites[4] especially under a large compressive stress. There have been several attempts to quantify the mechanical properties in radial direction of MWCNTs (Refs. 2, 5, and 6) and single wall CNTs (SWCNTs)[7] with atomic force microscopy (AFM). In such studies, a force versus deformation plot from the indentation measurement of CNT is readily acquired, and often a Hertzian contact model is applied to fit the experimental data and to extract the material properties of CNTs, especially the elastic modulus. Large variations in the measured elastic modulus of CNTs spanning from 0.3 to 80 GPa were reported.[2,5,6] However, it is well known that the Hertzian contact model is only suitable for modeling elastic deformations of small strain below several percentage, which limits the applicability of such a model analysis to indentation deformation of less than ~0.1 nm in the case of a SWCNT and ~1 nm in the case of a 10 nm diameter MWCNT. Accurately resolving the deformation behavior in such a small range is challenging even for the most advanced nanoindentation techniques.

In this work, we describe a study on the radial deformation of MWCNTs where a large reversible deformation up to the complete flattening was realized with AFM nanoindentation. The exact number of walls (thus the shell thickness) in this MWCNT, often uncertain in all previous studies, was also uniquely determined. A continuum shell model was subsequently applied to obtain the effective radial elastic modulus and to explain the linear and nonlinear deformation behaviors of the MWCNT. The use of an elastic shell model overcame the small strain requirement in the Hertzian analysis of indentation deformation in such hollow cylindrical nanotubes and allowed for the first time the full account of this significantly large elastic deformation of CNTs in nanoindentation.

II. EXPERIMENTAL

In this study, the MWCNTs used were synthesized by the arc discharge method and were dispersed on a Si substrate surface. A Dimension 3100 SPM with Nanoscope IV controller (Vecco, Inc.) operated at a controlled humidity level of below 10% was used throughout the experiment. For the nanoindentation study, a Si probe having a spring constant of ~3.5 N/m and a radius of curvature of ~60 nm (obtained from the deconvolution of the acquired AFM images of MWCNTs) was used, which was more than ten times larger than the radius of the studied MWCNT. The use of such a relatively large radius tip for the AFM nanoindentation on a nanostructure greatly lessened the effect of possible lateral sliding of AFM tip on measurement accuracy during the nanoindentation cycles and helped to maintain the mechanical engagement of the AFM tip on the nanostructure. Force-distance curves were first acquired from a rigid Si surface and used for indentation calibration. A fairly linear response was seen, implying the linearity of the AFM piezotube along the indentation direction. Under very low contact

[a)]Author to whom correspondence should be addressed. Electronic mail: mfyu@uiuc.edu.

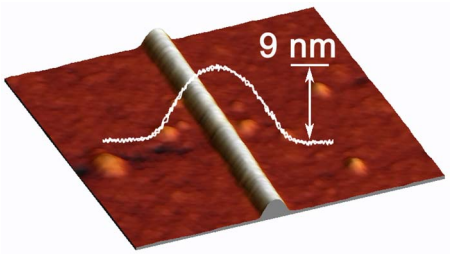

FIG. 1. (Color online) AFM topography image in three dimensional representation showing the MWCNT and the corresponding height profile acquired with AFM in contact mode. The scan size is 500 nm.

force, the probe tip was then directed toward a MWCNT and was symmetrically placed on top of its cylindrical geometry. Force-distance curves at a rate of 0.05 Hz were acquired multiple times at the same location. No obvious drift or creep was noticed in the duration of our measurement. The height profile of the MWCNT was immediately examined after acquiring each force-distance curve to verify the complete reversibility of the deformation.

III. RESULTS AND DISCUSSION

Figure 1 shows the three dimensional representation of the acquired AFM image from the studied MWCNT. The diameter of the MWCNT is determined to be ~9 nm based on the image acquired with minimal contact force in contact mode AFM. Force versus z distance data on a Si substrate surface and the MWCNT are shown in Fig. 2(a) (acquired data from two repeated loading and unloading cycles on the MWCNT were overlapped on each other to show the repeatability). Here, the z distance refers to the travel distance of the AFM piezotube along the indentation direction. On the hard Si substrate surface, the advance of the piezotube is fully converted to the deflection of the probe cantilever. Whereas on the MWCNT, a part of the piezotube motion is converted to the deformation of the MWCNT. Since the deformable MWCNT and the probe cantilever act as two springs in series, the actual deformation of the MWCNT can be simply obtained from the difference in z at the same applied force. Figure 2(b) shows the force-deformation curve constructed based on Fig. 2(a) by direct subtraction for the MWCNT. Four distinct responses were observed: (I) a linear deformation response extended up to ~3.7 nm indentation depth, which corresponds to ~40% of the outer diameter (OD) of the MWCNT, (II) one nonlinear deformation response showing approximately a power law dependence, (III) again a linear response, and (IV) finally a nondeformable response. The data presented are representative of ten cyclic measurements at different axial locations on the same MWCNT collected in a period over one month with different tips, demonstrating the reversible nature of even the most significant elastic deformation (up to ~60% of OD) in the MWCNT.

We reason that the observed deformation behavior reflects the evolution of the body geometry and the corresponding probe tip-elastic body interaction in such a hollow and cylindrical MWCNT undergoing local nanoindentation deformation, as illustrated in Fig. 3. The initial linear deformation region involves the radial deformation of the MWCNT having a circular cross section to an elliptical one; the intermediate nonlinear deformation region corresponds to the "bulb" formation and the extended flattening of the MWCNT in the axial direction. The second linear deformation region is due to the direct interaction between the probe tip surface and the bulbs, and the final nondeformable region shows the behavior of the completely flattened MWCNT (thus the graphite ribbon). Specifically, considering the evolution of the tip-sample contact area, in region (I), the contact area is mostly determined by the conformal deformation between a spherical indentation tip and a cylindrical sample, as in regular nanoindentation deformation of an elastic planar sample. In region (II), however, the evolution of the contact area deviates from this conformal deformation due to the limited deformation in the transversal direction and the extended deformation along the axial direction, a unique behavior of a cylindrical and hollow mechanical structure. In region (III), due to the significant flattening of the MWCNT under the tip and the bulb formation, the tip is instead in direct contact with the much rigid bulbs, and the contact area evolution is mainly limited by the deformation of such bulbs.

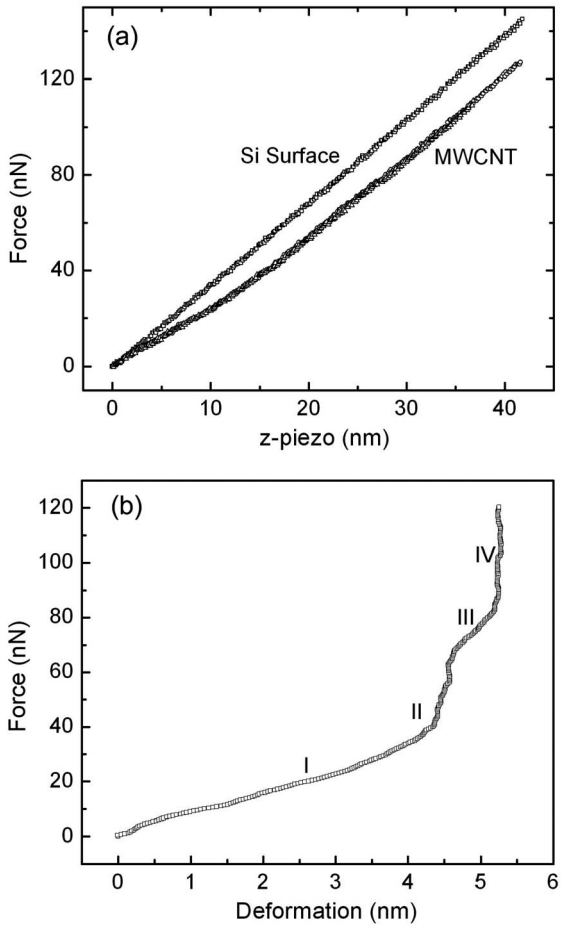

FIG. 2. (a) Force vs z distance curves acquired from a Si substrate surface and a MWCNT with AFM. The curve for the MWCNT includes data from two repeated measurements on the same location, showing the reversibility of the deformation. (b) Force vs deformation curve for the MWCNT constructed based on (a) by direct subtraction.

In the following, we first extract the exact number of walls in the studied MWCNT, thus the shell thickness, and

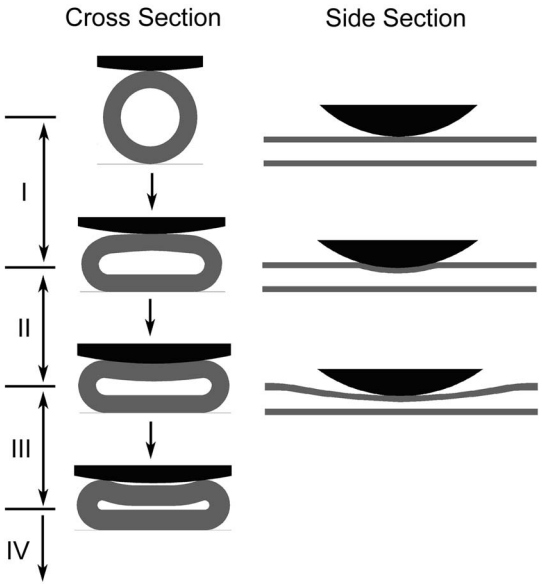

FIG. 3. Schematics illustrating the evolution of the cross sectional and side views of the MWCNT at different stages of nanoindentation with a spherical indenter.

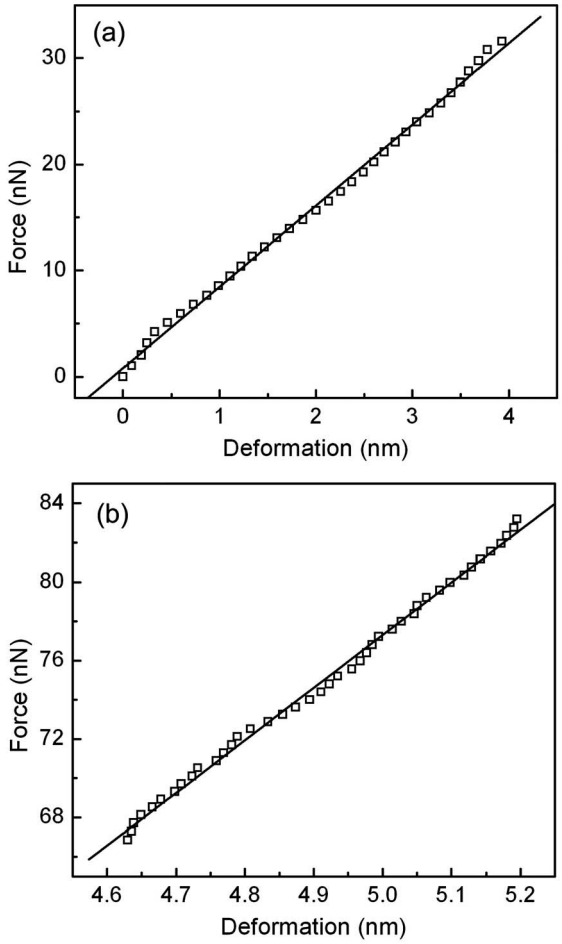

FIG. 4. The force-deformation curves corresponding to (a) the first linear deformation region and (b) the second linear deformation region acquired in the nanoindentation of MWCNT. The solid lines are the corresponding linear fits.

then apply the continuum shell model to analyze the observed deformation behavior. The number of walls n in the MWCNT can be obtained from the height (H_0 in nanometer) of the fully flattened configuration at the end of the nanoindentation, where n is the closest integer to $\frac{1}{2}(1+H_0/0.34)$, according to the interlayer distance of graphite, 0.34 nm. The height of the completely flattened MWCNT is determined from region (IV) in the acquired response curve. The diameter of the MWCNT is ~9 nm, the deformation in region (IV) is ~5.4 nm, and the height is thus ~3.6 nm. Here, n is calculated to be 6 and the shell thickness t for the MWCNT is then $0.34(n-1)$ (nm), ~1.7 nm.

Since the elastic property of a hexagonal graphite structure is isotropic,[8] and the chirality of CNT has little effect on its elastic property in radial direction,[9] we analyze the linear deformation of the MWCNT under nanoindentation with the elastic shell model by assuming a shell thickness of t and an elasticity modulus of E. In continuum shell theory, bending of a shell is always accompanied by in plane stretching. However, in some special cases, bending can occur without in-plane stretching, such as for a cylindrical shell with open ends.[10] Considering a cylindrical shell with open ends under a point load in radial direction, the deformation energy is then due to the bending in radial and axial direction, as illustrated in Fig. 3, and can be approximated as[11,12]

$$U = Et^3(d/R^2)^2Rl + Et(Rd/l^2)^2Rl, \quad (1)$$

where the first term is due to the radial bending and the second term is due to the deformation in the axial direction, E and t are the effective elastic modulus and the thickness of the shell, respectively, d is the indentation depth, and the axial deformation length $l \approx R\sqrt{R/t}$. Since this total energy is a harmonic function on indentation depth, the force-deformation response can be described by a linear function with an effective spring constant $k_I = \partial^2 U/\partial d^2$, as shown in Fig. 4. $k_I \sim cEt^{5/2}/R^{3/2}$, where $c \sim 1.2$ according to the finite element analysis.[11,12] The value of k_I for the MWCNT is obtained from linear deformation region (I) displayed in a zoomed view in Fig. 4(a) and is ~7.6 nN/nm, which yields an effective radial elastic modulus of $E \sim 16$ GPa for the MWCNT according to this shell model. This linear deformation behavior persisted up to twice the shell thickness, much like a classical homogenous shell described in continuum shell theory.[10] In the analysis, we have used the result of a point load deformation for a finite size tip in calculating the effective elastic modulus. Finite element analysis has shown that for this linear response, there is no significant difference between the point load solution and the finite tip size solution, and the effect of the tip size becomes evident only for larger deformation.[12]

As further indentation is introduced, the bulb formation along the edges of the deformed MWCNT begins to appear, which provides a strengthening effect to resist the shell deformation along the transversal direction of the MWCNT, but the deformation along the longitudinal (axial) direction continues. This results in the deviation of the indentation deformation from the linear behavior and thus the appearance of the nonlinear response in region (II). This nonlinear behavior therefore purely reflects the geometric effect in the

contact area evolution between the indentation tip and the deformed MWCNT surface. The change of this contact area is expected to be nonlinear in this region.[12]

The significant indentation (at an indentation depth of ~4.5 nm) eventually reaches to the stage that the MWCNT underneath the AFM tip is significantly squashed and two bulbs begin to form along the edge of the deformed MWCNT. Due to the finite size of the indentation tip, it begins to make contact with the bulbs, and the indentation force is mainly exerted on such rigid bulbs, as illustrated in Fig. 3. The deformation observed in the measurement reflects therefore the elastic deformation of these bulbs. By using elastic models for collapsed tubes, it has been shown[13] that the radius of the bulbs for a naturally collapsed CNT is on the order of $\sim(E_s/k)^{-1/2} \sim 0.8$ nm, where $E_s \sim 0.02$ eV Å^{-2} is the surface energy of graphite and $k \sim 1.4$ eV is the curvature modulus of CNT.[14] The indentation response in region (III) can then be approximated by considering the indentation deformation of two semicircular bulbs or, further, a full cylinder with an equivalent diameter. Taking the inner radius of the bulb to be 0.8 nm according to the above analysis, the outer diameter of the bulb or the equivalent cylinder is then ~5 nm. Assuming that the shell model is still applicable, the force-deformation response is again should be linear. According to the effective spring constant obtained from the slope of the corresponding response in region (III), as shown in Fig. 4(b), $k_{\mathrm{III}} \sim 26.8$ nN/nm, the estimated elastic modulus is then $E_{\mathrm{bulb}} \sim 24$ GPa. This value is close to, but slightly larger than, the value obtained from the first linear response. The deviation could be due to the simple assumption made in describing two semicircular bulbs or the application of the thin-shell model in the analysis. For a cylinder with a large t/R ratio, a thick-shell model is more appropriate.[12] However, the fundamentals of the proposed mechanics still hold.

It is expected that the MWCNT fully collapsed under the AFM tip at the final stage of nanoindentation. The response can then be approximated by considering the indentation deformation of a stack of graphene sheets. This can be estimated with the Sneddon model describing the indentation of a flat elastic surface with a spherical indenter,[15]

$$F = E/(1-\nu)[2\delta(\alpha^2 + R_{\mathrm{tip}}^2)/\alpha - 2R_{\mathrm{tip}}\alpha], \tag{2}$$

where δ and α are the indentation depth and the contact radius, respectively,

$$\delta = \frac{\alpha}{2}\ln\left(\frac{R_{\mathrm{tip}}+\alpha}{R_{\mathrm{tip}}-\alpha}\right).$$

For a maximum load of ~120 nN applied in this study, the contact radius is calculated to be ~3.8 nm. The average stress on the flattened MWCNT is then on the order of $\sigma_{\mathrm{av}} = F_{\mathrm{max}}/(\pi\alpha^2) \sim 2.6$ GPa. This, however, is expected to be an overestimation as the actual contact area should be larger considering that the flattening in the MWCNT only locally occurs underneath the AFM tip and the bulb formation still provides extra contact support to the AFM tip. Nevertheless, taking the elastic modulus of graphite along the direction perpendicular to the basal plane, $E = 36.5$ GPa and $\nu = 0.19$,[16] the maximum deformation induced under this stress is only ~0.2 nm, which is obviously not resolved in this study.

The contribution of the involved van der Waals forces to our indentation measurement is negligible. In the extreme case, the surface energy related to the van der Waals interactions between the layers of the collapsed innermost CNT is only 0.12 eV per unit length, $E_s\pi(R_i - r_i) = 0.12$ eV,[14] where r_i is the radius of the bulb, while the elastic energy associated with the curvature of the innermost CNT cylinder is ~1.6 eV, $\pi k/R_i = 1.6$ eV, where R_i is the inner radius of the CNT and k is the curvature modulus, and the energy associated with the bulb formation is ~5.5 eV. The change in elastic energy is much larger than the change in surface energy due to van der Waals interactions.

As was pointed out, the MWCNT elastically recovered after large deformation (up to 60%) in the subsequent repeated nanoindentation measurements [Fig. 1(a)]. Yu and coworkers have reported such a reversible elastic deformation in MWCNT up to ~40%. Shen *et al.*[6] have also observed such a behavior in a thick-walled MWCNT although in their case the recovery was not immediate and a vanishing residual deformation was present after unloading. However, in these previous studies, the related deformation behavior in nanoindentation was not fully resolved and elucidated. For a cylindrical shell structure under large deformation, one would expect to observe buckling in the force-deformation curve. However, in many measurements performed in this experiment, a drop in force, indicating the occurrence of buckling, was never observed. We attribute this finding to the multilayered nature of MWCNTs, as the occurrence of buckling in one layer is expected to be suppressed by the existence of other layers, similar to that in a multishelled cylindrical macrostructure.

IV. CONCLUSIONS

In summary, the reversible radial deformation of MWCNTs under AFM nanoindentation was studied. Different stages of deformation up to the complete flattening of MWCNT were resolved, the exact number of walls important for the quantitative description of the mechanics of MWCNT was determined, and the revealed deformation behaviors were fully explained. The shell mechanics model, as opposed to the Hertzian contact model, was used to extract the elastic modulus of MWCNT and was found to be sufficient to illustrate the observed large nanoindentation deformation. The study, besides showing the remarkable property of MWCNTs to undergo recoverable radial compression to significantly large extent, establishes also a general approach for the appropriate modeling of nanoindentation in such hollow and cylindrical nanostructures.

ACKNOWLEDGMENTS

The work is supported by the National Science Foundation under Grant No. CMMI 0600538.

[1] M.-F. Yu, O. Lourie, M. J. Dyer, K. Moloni, T. F. Kelly, and R. S. Ruoff, Science **287**, 637 (2000).
[2] V. Lordi and N. Yao, J. Chem. Phys. **109**, 2509 (1998); M.-F. Yu, T. Kowalewski, and R. S. Ruoff, Phys. Rev. Lett. **85**, 1456 (2000); **86**, 87 (2000); M.-F. Yu, M. J. Dyer, and R. S. Ruoff, J. Appl. Phys. **89**, 4554 (2001).

[3]R. S. Ruoff, J. Tersoff, D. C. Lorents, S. Subramoney, and B. Chan, Nature (London) **364**, 514 (1993).
[4]A. Cao, P. L. Dickrell, W. G. Sawyer, M. N. Ghasemi-Nejhad, and P. M. Ajayan, Science **310**, 1307 (2005).
[5]I. Palaci, S. Fedrigo, H. Brune, C. Klinke, M. Chen, and E. Riedo, Phys. Rev. Lett. **94**, 175502 (2005).
[6]W. Shen, B. Jiang, B. S. Han, and S. Xie, Phys. Rev. Lett. **84**, 3634 (2000).
[7]H.-Y. Wang, M. Zhao, and S. X. Mao, Appl. Phys. Lett. **89**, 211906 (2006).
[8]B. I. Yakobson, C. J. Brabec, and J. Bernholc, Phys. Rev. Lett. **76**, 2511 (1996); G. Cao, Y. Tang, and X. Chen, J. Nanoeng. Nanosyst. **219**, 73 (2005).
[9]S. Reich, C. Thomsen, and P. Ordejon, Phys. Rev. B **65**, 153407 (2002).
[10]L. D. Landau and E. M. Lifshitz, *Theory of Elasticity* (Pergamon, New York, 1986).
[11]P. J. de Pablo, I. A. T. Schaap, F. C. MacKintosh, and C. F. Schmidt, Phys. Rev. Lett. **91**, 098101 (2003).
[12]I. A. T. Schaap, C. Carrasco, P. J. de Pablo, F. C. MacKintosh, and C. F. Schmidt, Biophys. J. **91**, 1521 (2006).
[13]L. X. Benedict, N. G. Chopra, M. L. Cohen, A. Zettl, S. G. Louie, and V. H. Crespi, Chem. Phys. Lett. **286**, 490 (1998).
[14]N. G. Chopra, L. X. Benedict, V. H. Crespi, M. L. Cohen, S. G. Louie, and A. Zettl, Nature (London) **377**, 135 (1995).
[15]I. N. Sneddon, Int. J. Eng. Sci. **3**, 47 (1965).
[16]T. W. Ebbesen, *Carbon Nanotubes: Preparation and Properties* (CRC, New York, 1997).